Preparation and Performance Characteristics of Short-Glass-Fiber/Maleated Styrene–Ethylene–Butylene–Styrene/Polypropylene Hybrid Composites

Sie Chin Tjong,[1] Shi Ai Xu,[1,2] Robert Kwok Yu Li,[1] Yiu Wing Mai[3,4]

[1] *Department of Physics and Materials Science, City University of Hong Kong, Tat Chee Avenue, Kowloon, Hong Kong*
[2] *Institute of Polymer Science and Engineering, East China University of Science and Technology, 130 Meilong Road, Shanghai, China*
[3] *Centre for Advanced Materials Technology, University of Sydney, Sydney, NSW 2006, Australia*
[4] *Department of Manufacturing Engineering and Engineering Management, City University of Hong Kong, Tat Chee Avenue, Kowloon, Hong Kong*

Received 23 April 2001; accepted 10 October 2001

ABSTRACT: Eighty/twenty polypropylene (PP)/styrene–ethylene–butylene–styrene (SEBS) and 80/20 PP/maleated styrene–ethylene–butylene–styrene (SEBS-*g*-MA) blends reinforced with 30 wt % short glass fibers (SGFs) were prepared by extrusion and subsequent injection molding. The influence of the maleic anhydride (MA) functional group grafted to SEBS on the properties of SGF/SEBS/PP hybrid composites was studied. Tensile and impact tests showed that the SEBS-*g*-MA copolymer improved the yield strength and impact toughness of the hybrid composites. Extensive plastic deformation occurred at the matrix interface layer next to the fibers of the SGF/SEBS-*g*-MA/PP composites during impact testing. This was attributed to the MA functional group, which enhanced the adhesion between SEBS and SGF. Differential scanning calorimetry measurements indicated that SEBS promoted the crystallization of PP spherulites by acting as active nucleation sites. However, the MA functional group grafted to SEBS retarded the crystallization of PP. Finally, polarized optical microscopy observations confirmed the absence of transcrystallinity at the glass-fiber surfaces of both SGF/SEBS/PP and SGF/SEBS-*g*-MA/PP hybrid composites. © 2002 Wiley Periodicals, Inc. J Appl Polym Sci 86: 1303–1311, 2002

Key words: polypropylene (PP); fibers; compatibility; elastomers

INTRODUCTION

Polypropylene (PP) is widely used in industrial sectors because of its versatile properties and low cost. However, PP often fails in a brittle mode when subjected to impact loading, particularly at low temperatures. Accordingly, PP is blended with an elastomer to improve its impact performance. The incorporation of an elastomer into PP generally leads to a reduction in stiffness. Reinforcement by inorganic fillers or short glass fibers (SGFs) can restore the required stiffness and strength. The structure and mechanical properties of filler-reinforced PP/elastomer blends are well documented in the literature.[1–5] In general, the mechanical properties strongly depend on the interfacial adhesion of the filler and matrix, the dispersion of filler particles, the formation of core–shell morphology, and the processing conditions. Limited research has been conducted concerning the properties of glass-fiber-reinforced hybrid composites containing an elastomeric phase.

Nair et al.[6,7] studied the fracture resistance of glass-fiber-reinforced polyamide-6,6/ABS hybrids. They reported that the glass fibers promoted shear yielding of the matrix, thereby enhancing the fracture initiation and propagation resistance of the polyblends. Jancar[8] carried out a preliminary study on the effect of the elastomer content on the yielding and impact behavior of maleated PP/SGF/EPR hybrids. He reported that the Charpy notched impact strength of the composites at −20°C tended to increase with increasing EPR volume content. Moreover, large plastic deformation in the matrix and fiber interface and fiber pullout were the primary energy-dissipative processes during yielding and impact fracture.[8] Tam et al.[9] also reported similar findings, that fiber debonding and pullout were responsible for the impact failure of SGF/EPR/PP hybrids. However, they indicated that the elastomer exerted a limited toughening effect on the hybrids. The impact modifier had a strong toughening effect for the PP homopolymer only.[9]

The adhesion between the fiber and matrix or elastomeric phase plays a key role in determining the

Correspondence to: S. C. Tjong (aptjong@cityu.edu.hk).
Contract grant sponsor: Research Grants Council of the Hong Kong Special Administrative Region; contract grant number: CityU 1029/00E.

Journal of Applied Polymer Science, Vol. 86, 1303–1311 (2002)

mechanical properties of SGF-reinforced blends and hybrids. Nair et al.[7] indicated that the toughening effect caused by the glass fibers was critically related to the fiber–matrix interfacial strength. Toughening was observed in glass-fiber-reinforced nylon 6,6/ABS hybrids when the interface was strong. A functional group such as maleic anhydride (MA) is grafted to the polymeric matrix or SGF to enhance the interfacial adhesion of the composites.[8,10] It is thought that an elastomer functionalized with MA, such as maleated styrene–ethylene–butylene–styrene (SEBS-*g*-MA), can be employed to promote the interfacial adhesion of hybrids. SEBS-*g*-MA has been used increasingly in recent years to improve the compatibility and toughness of phase components of composites and polyblends. It serves as both a compatibilizer and an impact modifier.[11–14] Little information is available in the literature concerning the effect of SEBS-*g*-MA on the structure and properties of SGF-reinforced hybrids. For the successful application of SGF/SEBS-*g*-MA/PP hybrids in the industrial sector, mechanical properties such as the yield strength, stiffness, elongation, and impact strength and processing properties need to be optimized. In this study, we examined the morphology and thermal and mechanical properties of the SGF/SEBS-*g*-MA/PP hybrid composites.

EXPERIMENTAL

Materials

PP (Profax 6331) was purchased from Himont Co. (Thailand). Its density and melt-flow index were 0.9 g cm^{-3} and 12 g/10 min, respectively. Styrene–ethylene–butylene–styrene (SEBS; Kraton G1652) and SEBS-*g*-MA (Kraton FG 1901X) copolymers were kindly supplied by Shell Co. (Houston, TX). The copolymers had PS block and central ethylene–butylene (EB) block molecular weights of 7500 and 37,500, respectively, and a PS weight fraction of 28.6%. The MA content in Kraton FG 1901 X was 1.84 wt %.[15] SGFs approximately 4 mm long were used as reinforcements in this study.

Blending

All materials were dried separately in ovens for more than 48 h. The 80/20 (w/w) PP/SEBS and 80/20 (w/w) PP/SEBS-*g*-MA blends and their hybrids were prepared in a Brabender twin-screw extruder (Germany). The SGF content of the hybrids was fixed at 30 wt % (the glass-fiber content was based on the total mass of the polymers and SGF). The temperature profiles of the extruder were set at 180, 190, 220, and 220°C. After compounding, the extrudates were pelletized and then blended again in the extruder under the same conditions. The extruded strands were chopped into granules and dried at 100°C for 48 h. With these pellets, tensile bars (ASTM Standard D 638-91) and plaques (200 $\times$ 80 $\times$ 3.2 mm^3) were injection-molded with a Chen Hsong machine (Hong Kong). The barrel zone temperature profiles were set at 200, 210, and 220°C. For comparison, a 30/70 (w/w) SGF/PP composite was also injection-molded under similar conditions.

Morphology observations

Samples approximately 10 mm long were cut from the midsections of tensile bars and subsequently fractured in liquid nitrogen along the injection-molding direction. Samples containing SEBS copolymer were etched in a tetrahydrofuran (THF) solvent for 6 h so that the elastomeric particles from the matrix were dissolved. They were then washed with fresh THF and dried in an oven operated at 40°C. Finally, the surfaces were coated with a thin layer of gold before examination in a scanning electron microscope (JEOL JSM 820, Tokyo, Japan). Image analysis was used to determine the size of the elastomeric particles.

Mechanical measurements

An extensometer with a gauge length of 50 mm was used for the tensile test. Six specimens of each composition were tested, and the average value was recorded. Notched samples for Izod impact tests (ASTM Standard D 256) were cut from the injection-molded plaques. The tests were carried out with a CEAST pendulum impact tester (Italy) at 21°C. The fracture surfaces of the hybrid composites were also examined with scanning electron microscopy (SEM).

Thermal analysis

The crystallization behaviors of all samples prepared were studied with a differential scanning calorimeter (TA Instruments model 2910, Newcastle, DE). The samples were initially heated to 200°C and kept at this temperature for 5 min. They were cooled to 50°C at a scanning rate of 10°C/min and kept at this temperature for 5 min. Subsequently, they were heated to 200°C at the same rate. The data of first-cooling and second-heating processes were analyzed. Moreover, the spherulitic morphology of PP recrystallized from the melt was observed with a polarized optical microscope (Olympus BH2-UMA, Japan).

RESULTS AND DISCUSSION

Morphology

Figures 1 shows the typical fracture morphology of skin and core sections of the injection-molded 30/70

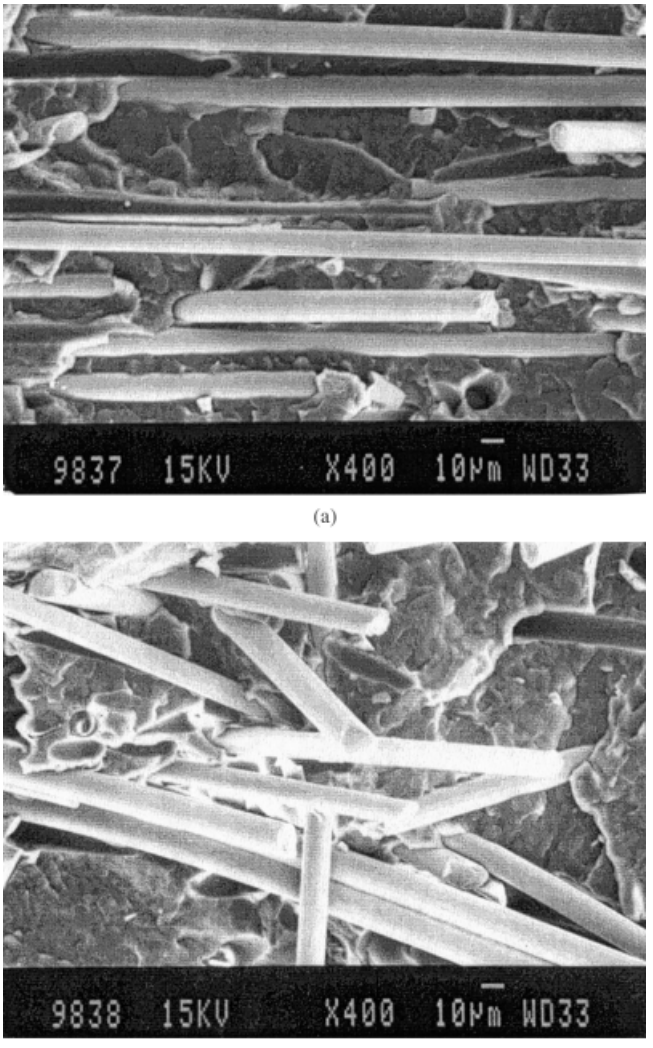

Figure 1 SEM micrographs showing fracture surfaces of (a) skin and (b) core sections of the 30/70 SGF/PP composite.

SGF/PP composite. Apparently, the glass fibers are aligned along the melt-flow direction in the skin layer of this composite. However, they orient randomly in the core section of the sample as expected [Fig. 1(b)]. Figure 2 presents SEM micrographs showing the fracture surfaces of skin sections of the SGF/SEBS/PP and SGF/SEBS-*g*-MA/PP hybrids. The interfacial bonding between the glass fibers and matrix of the SGF/SEBS/PP hybrid is relatively poor, as evidenced by clean fiber surfaces and fiber pullout behavior. In contrast, small pieces of materials are bonded firmly to the glass-fiber surfaces of the SGF/SEBS-*g*-MA/PP hybrid, indicating that a strong interfacial bond develops between the SGF and SEBS because of the incorporation of the MA functional group. The MA functional group is grafted to the central EB chain segment of the SEBS copolymer. Accordingly, the anhydride functional group grafted to EB can react with hydroxyl groups on the glass-fiber surfaces during compounding, thereby improving the compatibility between the SGF and SEBS. The reaction takes place between SEBS-*g*-MA and SGF as follows:

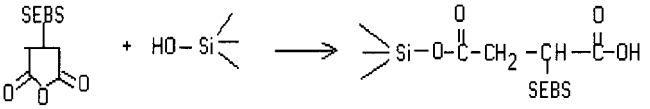

The elastomeric phase is reported to encapsulate the entire filler or glass-bead surface for maleated elastomer/PP hybrids reinforced with filler particles.[5] This leads to a fine dispersion of rigid particles with a core–shell structure within the PP matrix. However, elongated SGF can only result in a partial coating or bonding of fiber surfaces with thin layers of SEBS-*g*-MA [Fig. 2(b)].

There are different types of interfacial interactions that develop in the SGF/SEBS/PP and SGF/SEBS-*g*-

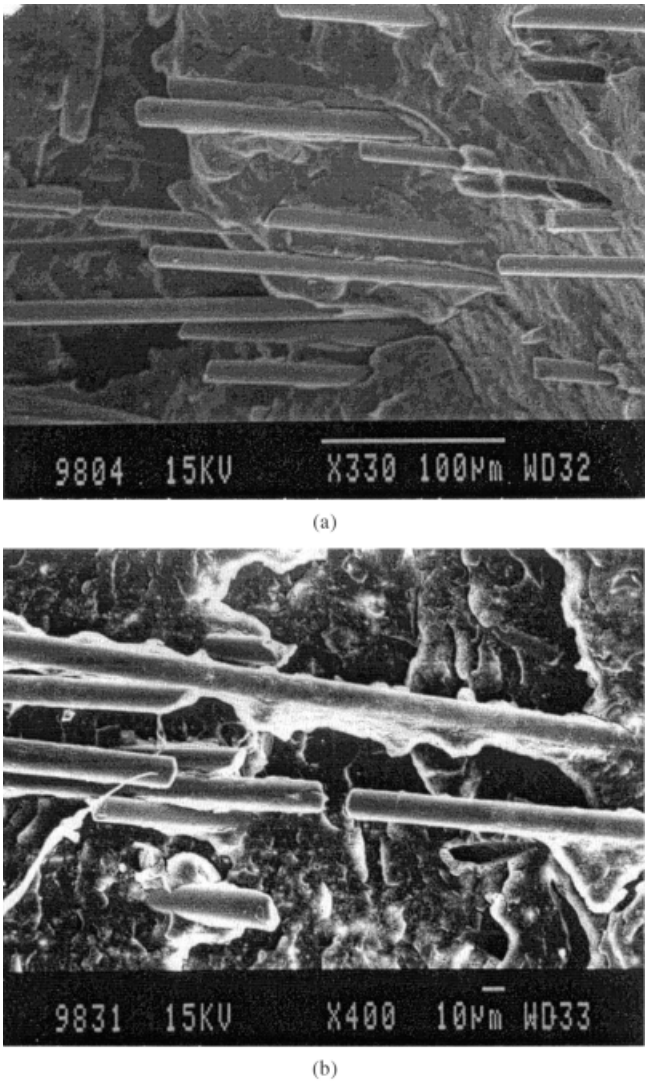

Figure 2 SEM micrographs showing fracture surfaces of skin sections of (a) SGF/SEBS/PP and (b) SGF/SEBS-*g*-MA/PP hybrids.

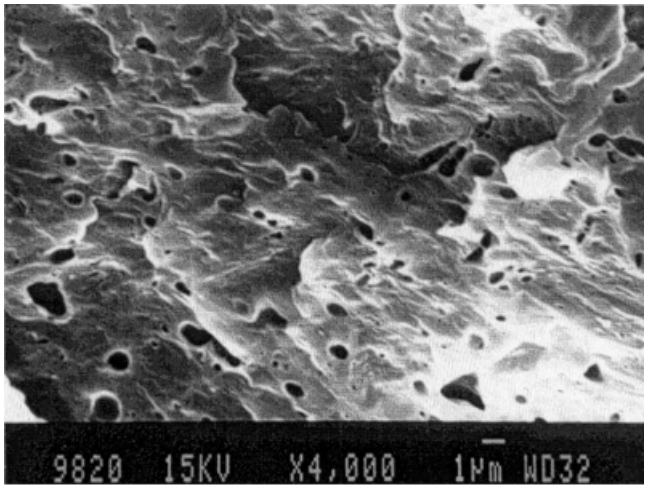

(a)

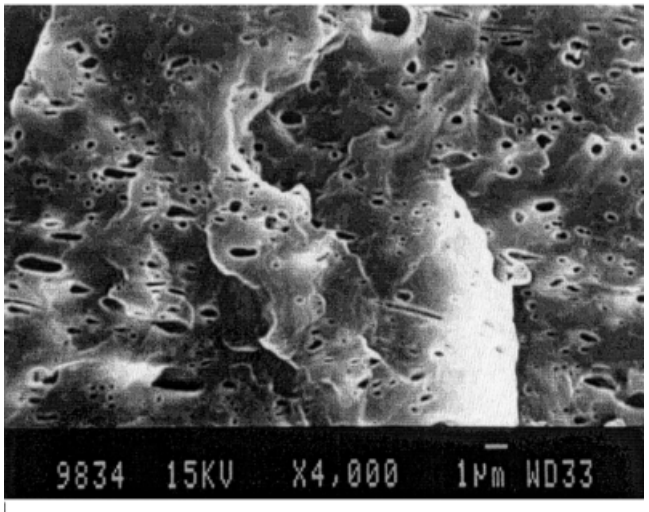

(b)

Figure 3 SEM micrographs showing the dispersion of SEBS particles in the matrices of (a) SGF/SEBS/PP and (b) SGF/SEBS-*g*-MA/PP hybrids. SEBS particles were extracted with THF.

MA/PP hybrids, that is, between SGF and SEBS (or SEBS-*g*-MA), between SGF and PP, and between PP and SEBS (or SEBS-*g*-MA). The interfacial bonding between SGF and SEBS can be improved with maleated SEBS, as discussed previously. The interaction between SGF and PP is limited because SGF has a polar surface and PP is a nonpolar polyolefin. As for PP and SEBS, a chemical interaction between them could exist, although PP and polystyrene are incompatible. This derives from the chemical structure of the midblock of SEBS being close to that of PP. Setz et al.[16] reported that SEBS had good compatibility with PP phases because SEBS could diffuse into the PP phase under the formation of micelles. The interdiffusion between the EB block of SEBS and PP increased the interfacial bonding.

Figure 3 presents high-magnification SEM micrographs showing the matrix morphology of SGF/SEBS/PP and SGF/SEBS-*g*-MA/PP hybrids. As elastomer particles are dissolved by THF, small voids associated with elastomer extraction can be seen to disperse within the matrix of hybrids. The size of the elastomeric particles of the SGF/SEBS-*g*-MA/PP hybrid (mean = 0.18 μm) is smaller than that of the SGF/SEBS/PP composite (mean = 0.48 μm) on the basis of image analysis.

Mechanical properties

Figure 4 shows the stress–strain curves for pure PP and its blends as well as hybrid composites tested at a crosshead speed of 10 mm/min. Apparently, PP homopolymer and SEBS/PP and SEBS-*g*-MA/PP binary blends exhibit typical ductile behavior. They undergo extensive plastic deformation up to a strain exceeding 910%, and no fracture is observed at this stage. The tensile behavior of the samples is characterized by the presence of a yield stress and necking followed by homogeneous drawing. Furthermore, stress whitening also occurs during the tensile deformation process. The incorporation of SEBS or maleated SEBS into PP leads to a sharp decrease in the yield stress. For restoration of the yield strength and stiffness, 30 wt % SGF is added to SEBS/PP and SEBS-MA/PP blends. According to Figure 1, SGF addition improves the yield stress of SEBS/PP and SEBS-MA/PP blends dramatically at the expense of tensile ductility. Therefore, the SGF maintains a stiffness–toughness balance of the SEBS/PP and SEBS-MA/PP blends. The tensile properties of all samples tested at a crosshead speed of 10 mm/min are summarized in Table I. The SGF/SEBS-MA/PP hybrid exhibits the highest yield stress among all samples investigated. Moreover, an improvement in tensile toughness is observed in the SGF/SEBS-*g*-MA/PP composite. The tensile toughness is defined in this study as the area of the stress–strain curves up to final failure. Accordingly, improvements in the tensile strength, stiffness, and toughness of the SGF/SEBS-*g*-MA/PP hybrid can be explained by the increased number of interactions between the SGF and maleated SEBS phase. According to Figure 3(b), maleated SEBS particles are embedded and dispersed within the PP matrix. Because strong adhesion exists between SGF and SEBS, it is thought that such interactions can promote stress transfer from the matrix to SGF during tensile loading.

The notched Izod impact toughness of pure PP and its blends as well as hybrid composites are listed in Table II. Apparently, PP homopolymer exhibits a very low impact toughness of 1.95 kJ/m^2 because PP is notch-sensitive under impact loading. Adding 30 wt % SGF to PP improves the impact toughness slightly. A maximum impact toughness of 17.78 kJ/mm^2 can be achieved by the blending of PP and SEBS as expected.

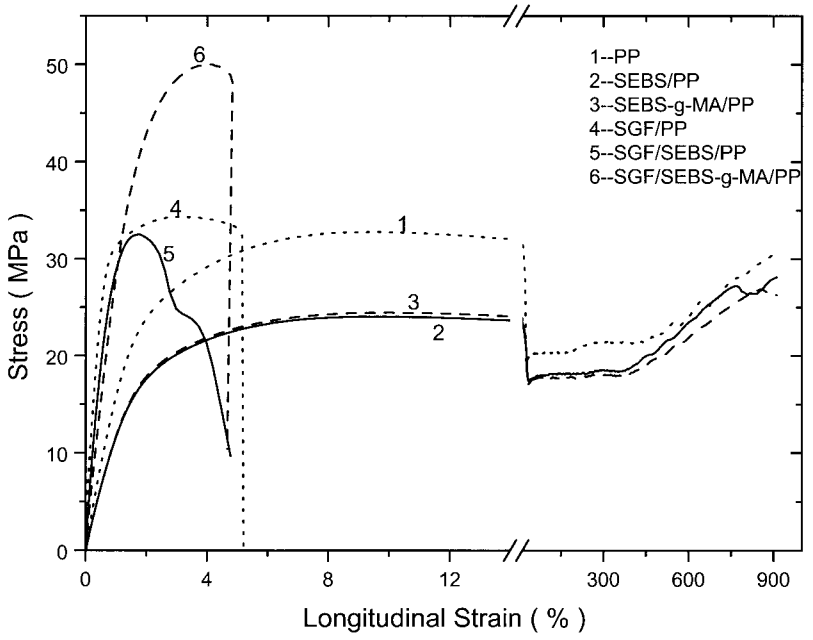

Figure 4 Stress–strain curves of all samples tested at 10 mm/min.

The further incorporation of SGF into SEBS/PP and SEBS-*g*-MA/PP blends leads to a sharp decrease in impact toughness. However, the impact toughness of the SGF/SEBS-MA/PP hybrid is higher than that of the SGF/SEBS/PP, SGF/PP, and PP samples. This is due to the functional MA group of SEBS, which interacts with the glass fiber during compounding, as discussed previously. Accordingly, the enhancements in the impact toughness observed for the SGF/SEBS-MA/PP hybrid are related to the better interfacial adhesion between the SGF and elastomeric phase. Nair et al.[7] reported that toughening in the glass-fiber-reinforced polyamide-6,6/ABS hybrid resulted directly from a strong interfacial bonding. It is thought that the SEBS layer can introduce a ductile interface between the SGF and PP matrix, leading to the occurrence of extensive plastic deformation in the SEBS interfacial layer during impact loading. Wu et al.[17] reported that the SEBS interface layer that formed at the wood-fiber/matrix region was beneficial in improving the impact toughness of PP hybrids because the SEBS layer could prevent the short fiber and PP matrix from premature brittle failure at the early stage of impact. The ductile SEBS layer also releases plastic constraint from the rigid fibers during impact testing, thereby inducing massive plastic deformation in the PP matrix. Figure 5 shows the fracture surface morphology of the SGF/SEBS/PP and SGF/SEBS-MA/PP hybrids after impact testing. Figure 5(a) reveals that the fibers on fractured surfaces are clean, and no matrix material adheres to their surfaces. The main features in this fractograph are the debonding and pull-out of fibers from the matrix of the hybrid. However, extensive plastic deformation occurs in both the bulk matrix and the interface matrix layer in the vicinity of glass fibers for the SGF/SEBS-*g*-MA/PP hybrid. Most glass fibers are bonded firmly to the matrix [Fig. 5(b)].

Crystallization behavior

The performance of thermoplastic composites depends mainly on the interfacial fiber–matrix bonding and on the crystalline properties of the matrix to a lesser extent.[18–21] The crystallization behavior and

TABLE I
Tensile Properties of PP and SEBS/PP Blends and Their Composites at a Crosshead Speed of 10 mm/min

Composition	Yield stress (MPa)	Stiffness (MPa)	Elongation at break (%)	Toughness (kJ/m^2)	Stress at break (MPa)
PP	32.6	1895	>910	>10,700	No fracture
SEBS/PP	24.1	1415	>910	>9,700	No fracture
SEBS-*g*-MA/PP	24.3	1391	>910	>9,500	No fracture
SGF/PP	34.4	5195	5.1	78	32.6
SGF/SEBS/PP	33.3	4251	3.9	43	19.5
SGF/SEBS-*g*-MA/PP	50.1	3346	5.0	88	48.5

TABLE II
Notched Izod Impact Results of PP and SEBS/PP Blends and Their Composites

Composition	Impact toughness (kJ/m^2)
PP	1.95
SEBS/PP	17.78
SEBS-*g*-MA/PP	16.72
SGF/PP	3.40
SGF/SEBS/PP	8.26
SGF/SEBS-*g*-MA/PP	9.63

nucleation of the semicrystalline PP phase in a composite reinforced with a filler could influence mechanical properties such as the tensile and impact strength.[20,22,23] Figure 6 shows differential scanning calorimetry (DSC) heating and cooling curves of PP and its blends as well as hybrid composites at 10°C/min. The results of DSC analyses are listed in Table III. The cooling curve of PP shows the presence of the crystallization exotherm [crystallization temperature (T_c)] at 116.4°C. T_c of PP remains nearly unchanged with the incorporation of SGF. However, the addition of nonmaleated SEBS increases T_c of PP to 119°C. This implies that SEBS accelerates the crystallization process by acting as a nucleating agent for PP. With MA grafted to SEBS, T_c is reduced to 117.3°C. As mentioned previously, the chemical structure of PP is close to that of the midblock of SEBS, and strong interfacial bonding exists between PP and SEBS.[16] However, grafting the MA functional group to SEBS increases the polarity of the central block. The compatibility between nonpolar PP and SEBS becomes poorer after maleation. Therefore, the functional MA group is ineffective in promoting the formation of crystallites in PP, as evidenced by a shift to a lower value of T_c and a low degree of crystallinity (X_c; see Table III). Finally, SGF has little effect on the crystallization of PP from the melt, and so the T_c value of the SGF/SEBS/PP hybrid composite is close to that of the SEBS/PP binary blend. Similar crystallization behavior is observed for the SGF/SEBS-MA/PP hybrid (Table III).

X_c of PP in its pure state and in the blends and composites is determined from the heat that evolves during the crystallization with the following relation:

$$X_c = \frac{\Delta H_c}{w \Delta H_m^o} \quad (1)$$

where ΔH_c is the heat of crystallization, ΔH_m^o is the heat of fusion for 100% crystalline PP, and w is the weight fraction of PP in the blends or composites. For pure PP, w is equal to 1. ΔH_m^o for PP is reported to be 209 J/g.[23] X_c values of PP for all the samples studied are also listed in Table III. Apparently, compounding SEBS with PP increases X_c, whereas SGF addition reduces X_c.

Figure 7 presents polarized optical microscopy (POM) micrographs showing the spherulitic morphology of PP, PP/SEBS, and PP/SEBS-*g*-MA blends after crystallization from the melt. The PP spherulites are characterized by a typical Maltese-cross extinction pattern. The spherulites become finer when PP is blended with SEBS but not when it is blended with maleated SEBS. Generally, large spherulites and slow crystallization in polyblends produce poor impact strength. It is apparent that these POM micrographs correlate well with the impact toughness of PP, PP/SEBS, and PP/SEBS-*g*-MA, as listed in Table II. It is worth mentioning that the spherulite morphology and crystallinity levels in PP are very sensitive to the thermal history of processing. Therefore, the prepared melt-crystallized samples may not illustrate the actual spherulite morphology of injection-molded samples.

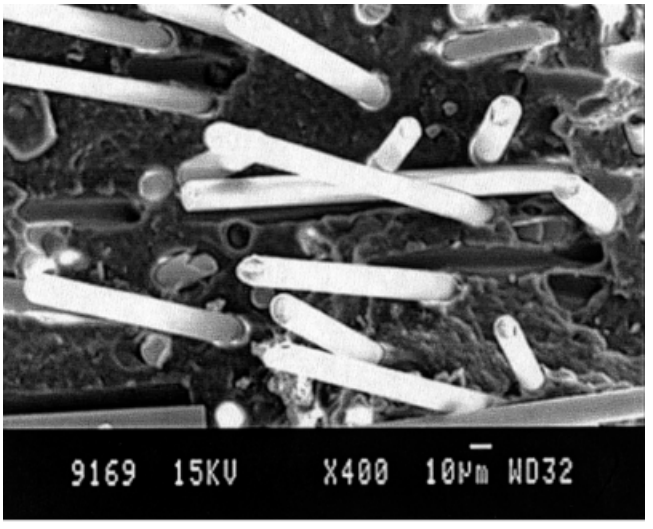

(a)

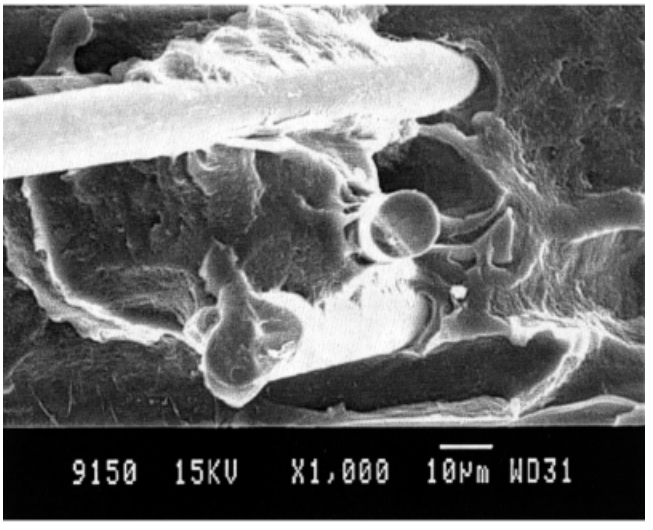

(b)

Figure 5 SEM micrographs of fracture surfaces of (a) SGF/SEBS/PP and (b) SGF/SEBS-*g*-MA/PP hybrids ruptured by impact testing.

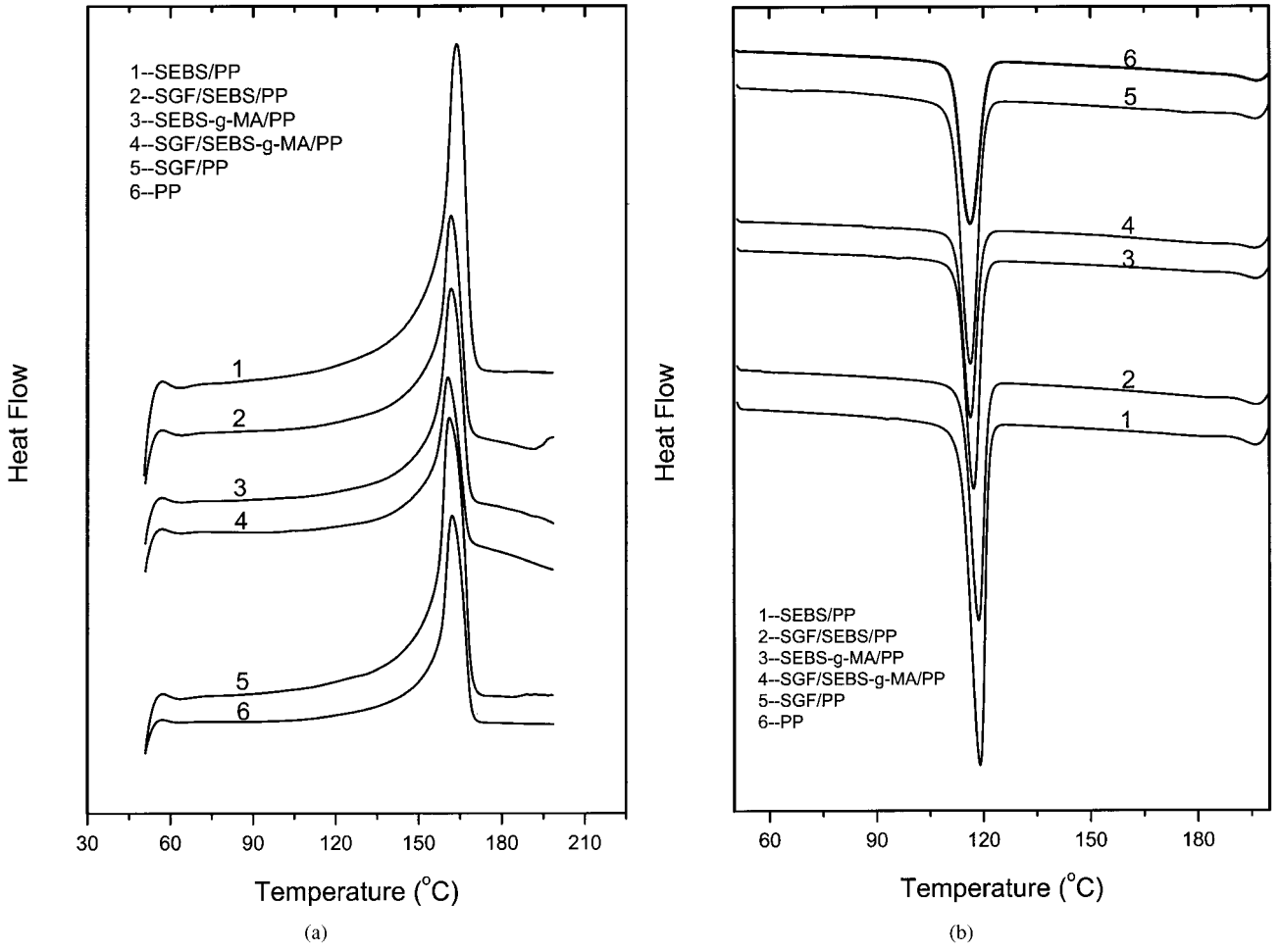

Figure 6 DSC curves showing (a) heating and (b) cooling behaviors of all samples at 10°C/min.

For glass-fiber-reinforced thermoplastic composites, the fiber surfaces generally favor heterogeneous nucleation by acting as nucleation sites for crystallization. If a high density of nucleation sites prevails, a columnar growth known as transcrystallinity will develop and enclose the fiber. Transcrystallinity can be induced in PP composites reinforced with fibers under the appropriate conditions.[22,24,25] Transcrystallinity at the fiber–matrix interface can facilitate stress transfer more efficiently. Figure 8 reveals that the glass fibers do not act as nucleation sites for PP spherulites in the composites. Moreover, the fibers do not induce transcrystallinity at their surfaces. As discussed previously, SGF has a polar surface, and PP is a nonpolar polyolefin; therefore, limited interaction occurs between them. Accordingly, crystallization only initiates in the bulk of the PP matrix. For samples containing SEBS, the elastomeric particles can act as nucleation sites for PP spherulites. In this case, the spherulites become smaller [Figs. 7(b) and 8(b)].

TABLE III
Melting Temperature (T_m), T_c, and X_c of All Investigated Samples

Composition	T_m (°C)	T_c (°C)	ΔH_c (J/g)	X_c (%)
PP	162.1	116.4	96.24	46.0
SEBS/PP	163.7	119.0	81.19	48.6
SEBS-*g*-MA/PP	161.8	117.3	76.79	45.9
SGF/PP	161.1	116.3	74.64	44.6
SGF/SEBS/PP	161.7	118.6	60.61	47.2
SGF/SEBS-*g*-MA/PP	160.8	116.3	60.18	46.8

CONCLUSIONS

SGF/SEBS/PP and SGF/SEBS-*g*-MA/PP hybrid composites were prepared by injection molding. The morphology and mechanical and crystallization behavior of the hybrids were investigated. Mechanical measurements indicated that the incorporation of maleated SEBS led to higher impact and yield strengths of the hybrid composites. This was attributed to the MA functional group improving the interfacial adhesion between SGF and SEBS. Extensive plastic deformation took place at the matrix interface layer in the vicinity of the fibers of the SGF/SEBS-*g*-MA/PP hybrid.

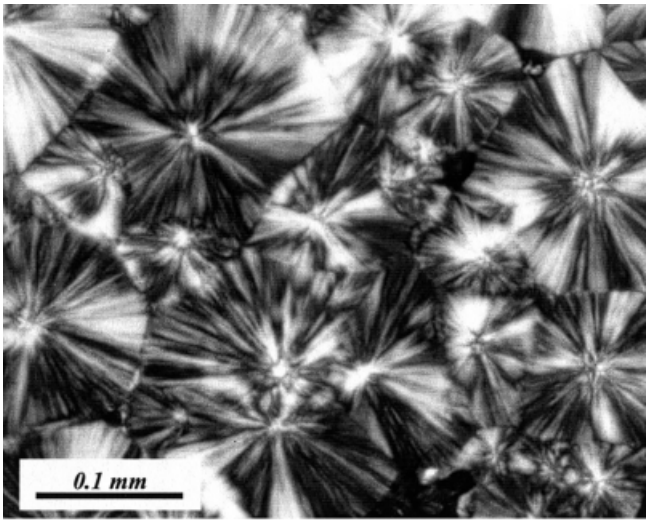

(a)

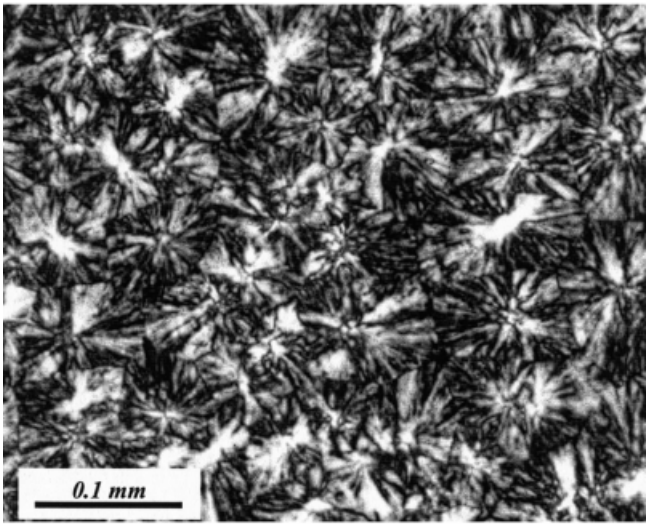

(b)

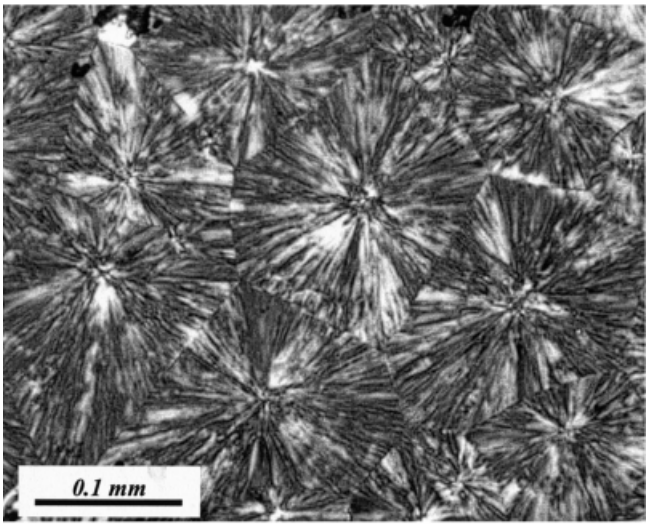

(c)

Figure 7 POM micrographs showing the spherulitic morphology of PP recrystallized from the melt: (a) pure PP, (b) 80/20 PP/SEBS, and (c) 80/20 PP/SEBS-*g*-MA.

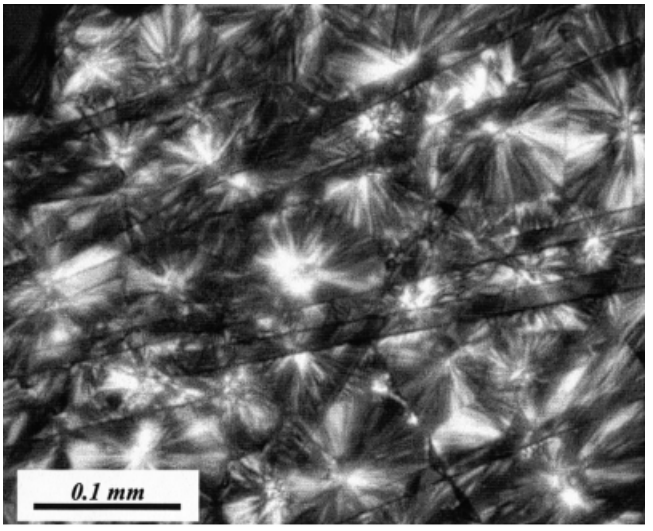

(a)

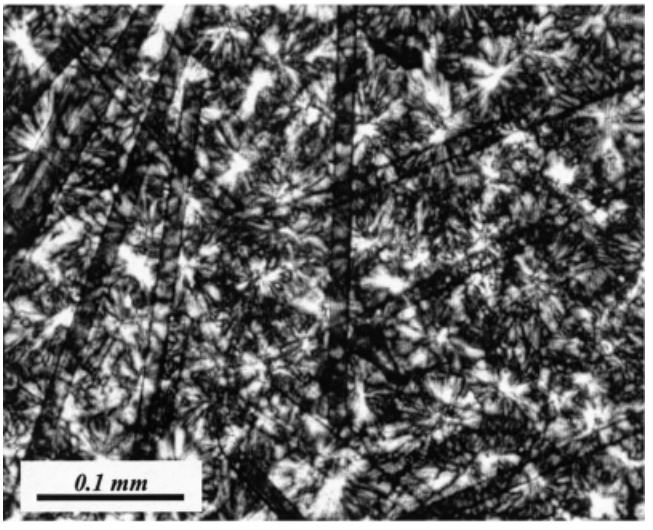

(b)

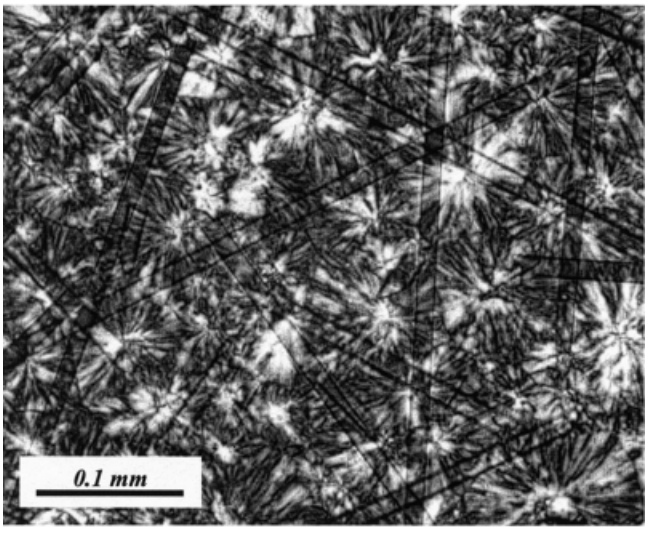

(c)

Figure 8 POM micrographs showing the spherulitic morphology of PP recrystallized from the melt: (a) SGF/PP, (b) SGF/SEBS/PP, and (c) SGF/SEBS-*g*-MA/PP.

Therefore, the mechanical performance of hybrid composites strongly depended on the adhesion at the fiber–matrix interface. SGF exerted a beneficial effect by maintaining a stiffness–toughness balance of the hybrid composites. From the results of DSC analyses and POM observations, SEBS enhanced the crystallization of PP spherulites by acting as potential nucleation sites. However, the MA functional group grafted to SEBS retarded the crystallization of PP. Finally, transcrystallinity was not observed at the glass-fiber surfaces of both hybrid composites.

References

1. Long, Y.; Shanks, R. A. J Appl Polym Sci 1996, 61, 1877.
2. Premphet, K.; Horanont, P. J Appl Polym Sci 2000, 76, 1929.
3. Stamhuis, J. E. Polym Compos 1994, 5, 202.
4. Tjong, S. C.; Xu, S. A. J Appl Polym Sci 2001, 81, 3231.
5. Liang, J. Z.; Li, R. K. Y.; Tjong, S. C. Polym Compos 1999, 20, 413.
6. Nair, S. V.; Subramaniam, A.; Goettler, L. A. J Mater Sci 1997, 32, 5335.
7. Nair, S. V.; Subramaniam, A.; Goettler, L. A. J Mater Sci 1997, 32, 5347.
8. Jancar, J. J Mater Sci 1996, 31, 3983.
9. Tam, W. Y.; Cheung, T. Y.; Li, R. K. Y. J Mater Sci 2000, 35, 1525.
10. Zhou, X.; Dai, G.; Guo, W.; Lin, Q. J Appl Polym Sci 2000, 76, 1359.
11. Wong, S. W.; Mai, Y. W. Polym Eng Sci 1999, 39, 356.
12. Wong, S. W.; Mai, Y. W. Polymer 1999, 40, 1553.
13. Kim, G. M.; Michler, G. H.; Rosch, J.; Mulhaupt, R. Acta Polym 1998, 49, 88.
14. Tjong, S. C.; Xu, S. A. J Appl Polym Sci 1998, 68, 1099.
15. Oshinski, A. J.; Keskukula, H.; Paul, D. R. Polymer 1992, 33, 268.
16. Setz, S.; Stricker, F.; Kressler, J.; Duschek, T.; Mulhaupt, R. J Appl Polym Sci 1996, 59, 1117.
17. Wu, J.; Yu, D.; Chan, C. M.; Kim, J.; Mai, Y. W. J Appl Polym Sci 2000, 76, 1000.
18. Roux, C.; Denault, J.; Champagne, M. F. J Appl Polym Sci 2000, 78, 2047.
19. Tjong, S. C.; Xu, S. A. Polym Int 1997, 44, 95.
20. Park, C. S.; Lee, K. J.; Nam, J. D.; Kim, S. W. J Appl Polym Sci 2000, 78, 576.
21. van der Wal, A.; Mulder, J. J.; Gaymans, R. J. Polymer 1998, 39, 5477.
22. Ismail, Y. S.; Richardson, M. D.; Olley, R. H. J Appl Polym Sci 2001, 79, 1704.
23. Wurdelich, B. Thermal Analysis; Academic: New York, 1990; p 418.
24. Wang, C.; Liu, C. R. Polymer 1997, 38, 4715.
25. Tjong, S. C.; Chen, S. X.; Li, R. K. Y. J Appl Polym Sci 1997, 64, 707.